Applied Magnetic Resonance
https://doi.org/10.1007/s00723-018-1030-1

Applied
Magnetic Resonance

ORIGINAL PAPER

Impurities of [1-^{13}C]Pyruvic Acid and a Method to Minimize Their Signals for Hyperpolarized Pyruvate Metabolism Studies

Talia Harris[1] · Ayelet Gamliel[1] · Jacob Sosna[1] · J. Moshe Gomori[1] · Rachel Katz-Brull[1]

Received: 19 February 2018 / Revised: 23 May 2018

Abstract
Impurities are a necessary evil when working with hyperpolarized [1-^{13}C]pyruvate for real-time metabolic studies. We show that the impurities' spectrum persists throughout the detection window as these signals show a long T_1. At the same time, the impurities' spectrum is unpredictable and partly susceptible to minute pH changes in the microenvironment such that impurities' signals may overlap with hyperpolarized metabolite signals. We show a method to eliminate the hyperpolarized impurities' signals while maintaining sufficient hyperpolarized [1-^{13}C]pyruvate signal for metabolic studies.

1 Introduction

The development of the dissolution dynamic nuclear polarization (dDNP) technology by Ardenkjaer-Larsen et al. [1] revolutionized the field of metabolic nuclear magnetic resonance (NMR) studies in living systems by improving liquid state NMR signals by 3–4 orders of magnitude [1]. Since then many compounds—such as glutamate [2], fumarate [3], lactate [4], glucose [5], fructose [6], acetate [7], choline [8, 9], and bicarbonate [10]—have been hyperpolarized and their metabolism has been characterized in biological systems. Surprisingly, the initial compound described in the first in vivo metabolic study in 2006 [11], [1-^{13}C]pyruvic acid, has shown robustness in many systems and is still the most common hyperpolarized metabolic marker in use today [12–15]. It has also been used in the (only) three hyperpolarized clinical studies published to date [16–18].

The presence of small amounts of impurities in neat pyruvic acid is well documented and may be the result of the synthesis process and/or storage conditions

✉ Rachel Katz-Brull
rkb@hadassah.org.il

[1] Department of Radiology, Hadassah-Hebrew University Medical Center, POB 12000, 9112001 Jerusalem, Israel

Published online: 29 June 2018

[19–23]. Although care can be taken in sample synthesis and storage to minimize the impurity content, [1-^{13}C]pyruvic acid is a reactive compound and it will be virtually impossible to prevent formation of any impurities. When [1-^{13}C]pyruvic acid is hyperpolarized, the ^{13}C labeled sites of these impurities will be enhanced as well, and if they possess a sufficiently long T_1, will be observed in the hyperpolarized spectra. These pyruvic acid impurities can interfere with hyperpolarized [1-^{13}C] pyruvate metabolism studies as the exceptional sensitivity of dDNP enables observation of metabolic products whose concentration, like the impurities, is 2–3 orders of magnitude lower than pyruvate's. The presence of such impurities has been mentioned anecdotally in previous studies [24–26]. Recently, Duwel et al., have identified one such impurity as [1,5-^{13}C]zymonic acid and identified its potential as a pH marker, either as a purified compound in vivo or from the trace impurity in [1-^{13}C] pyruvic acid [27, 28]. Perkins et al. [29] have shown that aqueous solutions of pyruvic acid contain, in addition to pyruvic acid and pyruvic acid hydrate, five different tautomers and hydrates in equilibrium, namely, parapyruvic acid (diol), parapyruvic acid (ketone), zymonic acid (ketone), zymonic acid (diol), and zymonic acid (enol).

We show here that hyperpolarized [1-^{13}C]pyruvate impurity spectra observed in batches of [1-^{13}C]pyruvic acid obtained from two different manufacturers comprise signals that may be attributed to the same five tautomers and hydrates of these dimers of [1-^{13}C]pyruvic acid. For both batches, we characterize the chemical shifts and longitudinal relaxation times of these pyruvate impurities at several pH values in the physiological range and demonstrate the potential overlap with [1-^{13}C]pyruvic acid metabolite signals. Finally, we demonstrate the utility of incorporating a bloc of frequency selective excitations to hyperpolarized [1-^{13}C]pyruvic acid metabolism experiments in significantly decreasing the intensity of the pyruvate impurities' signals in the relevant chemical shift range with minimal effect on the [1-^{13}C]pyruvate signal itself, i.e., with minimal effect on the ability to monitor the metabolic conversions of [1-^{13}C]pyruvate.

2 Materials and Methods

2.1 Chemicals

The OXO63 radical (GE Healthcare, UK) was obtained from Oxford Instruments Molecular Biotools (Oxford, UK). [1-^{13}C]pyruvic acid was purchased from Sigma-Aldrich (SA, Rehovot, Israel) and from Cambridge Isotope Laboratories (CIL, Tewksbury, MA, USA).

2.2 DNP Spin Polarization and Dissolution

Spin polarization and fast dissolution were carried out in a dDNP spin polarization device (HyperSense, Oxford Instruments Molecular Biotools, Oxford, UK) operating at 3.35 T. Microwave frequency of 94.110 GHz was applied for the polarization of a [1-^{13}C]pyruvic acid formulation at 1.40–1.49 K. The formulations consisted of

11.1–14.0 mM OX063 radical in the neat acid. The amount of [1-^{13}C]pyruvic acid formulation placed in the polarization cup was 5 ± 0.5 mg. The dissolution process was performed as previously described [1]. The amount of pyruvic acid placed in the polarization cup was quickly dissolved in 4 ml of superheated aqueous media (170 °C and 10 bar). The dissolved hyperpolarized solution was directly injected to a screw cap 10-mm NMR tube in a 5.8-T NMR spectrometer via a PTFE line of about 2.4 m length with 6 s of He (g) chase. The dissolution medium consisted of 4 ml of 50 mM phosphate buffer which contained 19 mM TRIS and 138.6 mM NaCl. The pH of the dissolution medium was adjusted with NaOH such that upon mixing with the pyruvic acid in the cup the final pH reached the desired value. Following dissolution, the pH of the solution was determined.

2.3 NMR Spectroscopy

^{13}C NMR spectroscopy was performed in a 5.8-T high resolution NMR spectrometer (RS2D, Mundolsheim, France) using a 10-mm broadband NMR probe. For the measurements of hyperpolarized [1-^{13}C]pyruvate impurities in solution, non-selective ^{13}C spectra were acquired with a 15° nutation angle and a repetition time of 5 s. The bandwidth was selected to detect the entire spectral width of the ^{13}C spectrum (300 ppm) enabling simultaneous detection of hyperpolarized [1-^{13}C]pyruvate and its impurities. Acquisition of ^{13}C spectra was initiated prior to arrival of the hyperpolarized sample in the NMR tube and continued for more than 4 min after its arrival. For thermal equilibrium observation of the impurities' signals, the spectra were recorded with a 50° excitation angle and repetition times of 15–30 s for 2–4 days. For the suppression of hyperpolarized impurity signals in solution, selective excitations were acquired by applying a 2.5-ms sinc pulse centered at 179.8 ppm every 0.5 s. This pulse applied ca. 90° excitation to [1-^{13}C]pyruvate hydrate, ca. 5° to [1-^{13}C]pyruvate, and $>40°$ excitation in the 175–183 ppm range (see Fig. 6 for excitation profile).

For the perfused ex vivo rat brain slices, spectra were acquired using selective excitations by applying a 3-ms sinc pulse centered at 179.8 ppm that applied ca. 90° excitation to [1-^{13}C]pyruvate hydrate, ca. 5° to [1-^{13}C]pyruvate, and $>40°$ excitation in the 174–184 ppm range. Approximately 5 s after the arrival of hyperpolarized [1-^{13}C]pyruvate, four spectra were acquired rapidly with a repetition time of 1 s, to depolarize the impurity signals. Subsequently, spectra were acquired every 21 s to observe the hyperpolarized metabolic products that were building up with a high signal-to-noise ratio.

2.4 Spectral Processing and Data Analysis

Spectral processing was performed using MNova (Mestrelab Research, Santiago de Compostela, Spain). Baseline correction and calculation of integrated intensities were performed either with MNova or with DMFIT [30].

Determination of the T_1 of the hyperpolarized sites was performed by simulating the effect of repeated excitations and longitudinal relaxation on the signal integrals according to the following equation: $M(t) = M_0 \times e^{\left(\frac{-t}{T_1}\right)} \times \cos\theta^{\left(\frac{t}{TR}\right)}$ in

which TR, the time between excitations is known and θ is the excitation angle. As sample turbulence throughout the hyperpolarized acquisition window precluded directly determining the T_1 from the applied angle of excitation, as it assumes a static sample, we determined the effective angle of excitation, θ_{eff}, by fixing the T_1 of [1-^{13}C]pyruvate at 65 s, based on prior measurements in the same spectrometer. Effective angles of excitation between 8.5°–12° were found. Using the resultant θ_{eff}, the T_1s of the other sites were determined.

2.5 Demonstration of the Utility of the Bloc of Frequency Selective Excitations in a Metabolic Investigation

A set-up of ex vivo viable rat brain slices has been developed in our lab for investigating brain metabolism with metabolic substrates administered in a hyperpolarized state. The approach for quenching hyperpolarized signals of pyruvate impurities developed here was found to be useful for this type of studies. For this reason, a brief description of the brain slices methodology and one example is given here, although the entire study will be described elsewhere.

2.6 Artificial Cerebrospinal Fluid (aCSF) and a Perfusion System

The artificial cerebrospinal fluid (aCSF) used for slice perfusion contained 125 mM NaCl, 2.5 mM KCl, 15 mM D-glucose, 26 mM $NaHCO_3$, 1 mM $MgCl_2$, 1.25 mM NaH_2PO_4, and 2 mM $CaCl_2$ in water (90/10 v/v double-distilled H_2O/D_2O). The medium was bubbled with 95%/5% O_2/CO_2 for 1 h prior to slice perfusion and continuously bubbled with this gas mixture throughout the experiment at a flow rate 0.4 l/min. The pH of the medium was 7.4. A 200 ml reservoir of this aCSF was kept in a water bath at 40 °C outside the NMR spectrometer and was delivered to the NMR tube with a peristaltic pump at a rate of 4 ml/min. The temperature of the slices during the perfusion inside the NMR spectrometer was 32 °C. The temperature was calibrated independently with a thermocouple prior to each experiment.

2.7 Animal

A female Sprague–Dawley rat (ca. 4 months old and ca. 150 g) was obtained from the Hebrew University Authority of Biological and Biomedical Models. All the experimental procedures were in accordance with the regulations of the Institutional Animal Care and Use Committee of the Hebrew University. The animal was anesthetized with isoflurane using a gas anesthesia system (Somnosuite, Kent Scientific, Torrington, CT, USA). For induction, we used 3.5% isoflurane and 440 ml/min of room air. For maintaining anesthesia, we used 2.8–3.0% isoflurane and the same air flow.

2.8 Surgical Procedure and Slice Preparation

The surgical procedure began after obtaining a negative pedal pain reflex. First, the diaphragm was exposed by a subcostal incision. Then, it was removed to allow view of the heart. The right atrium was then cut to allow drainage of blood and 30 ml of ice-cold aCSF were injected into the left ventricle over ca. 5 min, taking care not to allow the passage of air bubbles to the heart and circulation. This procedure was done to wash blood away from the brain prior to the brain extraction and slicing. The animal was then sacrificed by decapitation. The brain was rapidly removed and placed into ice cold aCSF (~ 1–2 °C). The cerebrum was separated from the cerebellum and whole cerebrum precision cut slices (500 µm) were prepared using a McIlwain tissue chopper (The Mickle Laboratory Engineering Company Ltd., Surrey, UK). The process of brain extraction and slicing of the entire cerebrum took about 30 min from the moment of decapitation. Throughout this time, the tissue was constantly kept in the ice cold aCSF.

2.9 Experimental Design: Hyperpolarized Media Injection and Work Flow

To perform hyperpolarized experiments, it is important to be able to rapidly inject a small volume of hyperpolarized solution directly to the brain slices. The hyperpolarized solution was injected to the very bottom of the NMR tube containing the slices, within 15 s from the start of the dissolution process. The greenish color of the radical solution enabled visual inspection of the resulting solution (after the measurement) and ensured the homogenous distribution of the hyperpolarized media around the brain slices in the NMR tube. The hyperpolarized media was injected gently to minimize tissue displacement and care was taken to avoid the introduction of air bubbles. Immediately prior to the hyperpolarized medium injection (ca. 30 s), the perfusion was stopped, and was resumed only after acquisition of hyperpolarized spectra was completed (approximately 4 min). This was done to characterize the metabolism of a constant concentration of [1-^{13}C]pyruvate without the effects of wash-in and wash-out. In the particular example shown here, the slices were incubated for 2 h with 30 mM ethanol prior to the hyperpolarized [1-^{13}C]pyruvate administration.

3 Results

Upon dissolution of hyperpolarized [1-^{13}C]pyruvic acid in phosphate buffer to a final concentration of 14 ± 1 mM (pH 7.14–7.15), the peaks of [1-^{13}C]pyruvate (Fig. 1a (1), 171.0 ppm) and its equilibrating hydrate (Fig. 1a (2), 179.2 ppm) can be clearly seen. Upon closer examination of the spectra, many other peaks can be observed as well (Fig. 1b, c). The two peaks at 205.5 and 206.5 ppm (Fig. 1b (4) and (3), respectively), can be assigned to the natural abundance ^{13}C of C_2-pyruvate that appears at 206.0 ppm and is split to a doublet due to the labeling of the C_1-pyruvate position ($J = 62$ Hz). Similarly, the peaks observed at 170.5 and 171.5 ppm (Fig. 1b (6) and (5), respectively) can be assigned to

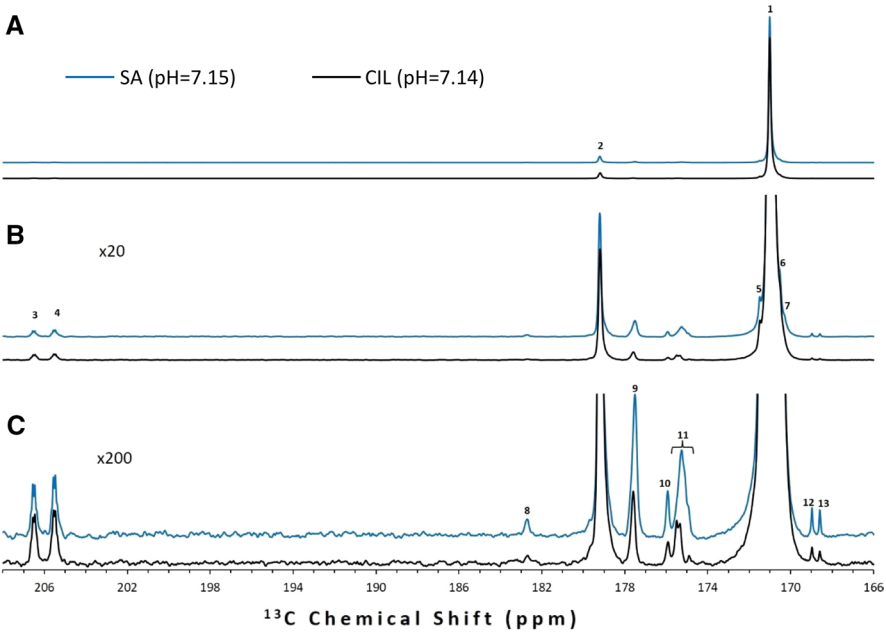

Fig. 1 ^{13}C-NMR spectra of hyperpolarized [1-^{13}C]pyruvate from two different suppliers. In blue and black (top and bottom on each panel, respectively): [1-^{13}C]pyruvic acid supplied by Sigma-Aldrich (SA) and Cambridge Isotopes Laboratories (CIL), respectively. **a** The chemical shift region of [1-^{13}C]pyruvate and [1-^{13}C]pyruvate-hydrate with intensity scale set to view the full [1-^{13}C]pyruvate signal. **b** The same spectra and spectral window shown in **a**, zoomed 20-fold to provide visibility of the signals that fall very close to the [1-^{13}C]pyruvate signal (while the [1-^{13}C]pyruvate and the [1-^{13}C]pyruvate-hydrate signals are truncated). Assignments: 3 and 4—C_2 of [1-^{13}C]pyruvate; 5 and 6—satellites of [1-^{13}C]pyruvate; 7—impurity of the SA formulation. **c** The same spectra and spectral window shown in **a**, zoomed 200-fold to provide better visibility of the impurity signals not overlapping the main [1-^{13}C]pyruvate signal, marked 8, 9, 10, 11, 12, and 13

the C_1-pyruvate satellites. Other than these peaks, multiple additional impurity peaks can be observed in the two formulations: an impurity peak is observed at 170.3 ppm (Fig. 1b (7)) in one of the formulations; impurity peaks at 182.7, 177.5, and 175.9 ppm (Fig. 1c (8), (9), and (10), respectively) can be observed in both formulations; Between 174.9 and 175.8 ppm (Fig. 1c (11)) multiple impurity peaks can be observed in both formulations. It seems that the impurities in both commercial formulations are somewhat similar (Fig. 1c), however, their relative signal intensities appear to be different with some possible changes in chemical shift (which could reflect differences in composition).

Following the careful characterization of Perkins et al. [29] of the compounds observed in a distillate of pyruvic acid, it appears that the impurities observed here, in a hyperpolarized state, in batches of two different suppliers, show signals due to the same species identified in the Perkins et al. study—namely [1,5-$^{13}C_2$] zymonic acid in the enol as well as the ketone and/or diol forms and [1,5-$^{13}C_2$] parapyruvic acid in the ketone and diol forms (Fig. 2).

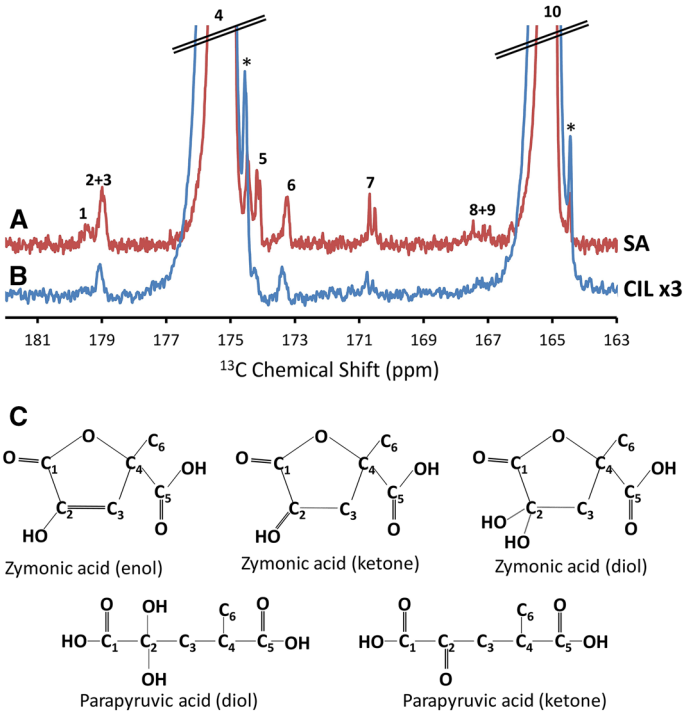

Fig. 2 ^{13}C-NMR thermal equilibrium spectra of **a** 230 mM of SA [1-^{13}C]pyruvic acid (8000 scans) and **b** 260 mM of CIL [1-^{13}C]pyruvic acid (12,800 scans) in 90%H_2O/10%D_2O and measured with 50° excitation angle and repetition times of 15–30 s. The spectra were normalized to the intensity of C_1-pyruvate and after normalization the CIL spectra is displayed multiplied by a factor of 3 to better observe the impurity peaks. The C_1-pyruvate and C_1-pyruvate hydrate signal were truncated to better observe the lower intensity peaks. The signals marked with an asterisk are the satellite signals C_1-pyruvate and C_1-pyruvate hydrate. Due to the asymmetry of the line shape only the low field satellite signal could be observed. According to Perkins et al. [29], the assignment of the signals observed here is likely as follows: 1. C_5-parapyruvic acid (diol), 2. C_5-parapyruvic acid (ketone), 3. C_5-zymonic acid (ketone), 4. C_1-pyruvic acid (hydrate), 5. C_1-zymonic acid (diol), 6. C_5-zymonic acid (enol), 7. C_1-zymonic acid (enol), 8. C_1-parapyruvic acid (ketone), 9. C_1-zymonic acid (ketone), 10. C_1-pyruvic acid. The structure and carbon numbering of these tautomers and hydrates are given in the lower panel scheme

Excluding the region ± 1 ppm from [1-^{13}C]pyruvate, we found that 1.1 ± 0.2% (n = 4) and 2.3 ± 0.1% (n = 4) of the hyperpolarized signal is present in impurities in the CIL and SA formulations, respectively. These limits on the percentage of impurities in each batch were calculated using four different samplings of the same batch at four different pH values. The distribution of these relative signal intensities is shown in Fig. 3. To further characterize the potential effect of such impurities on metabolic studies, we were interested in observing the pH dependence of their chemical shift. It can be seen in the SA formulation that even in the very narrow physiological range observed (pH 6.96–7.51), while several impurity signals are insensitive to pH changes (Fig. 4a, peaks marked with dotted lines) other impurity signals appear very sensitive, displaying more than 1 ppm changes in chemical shift

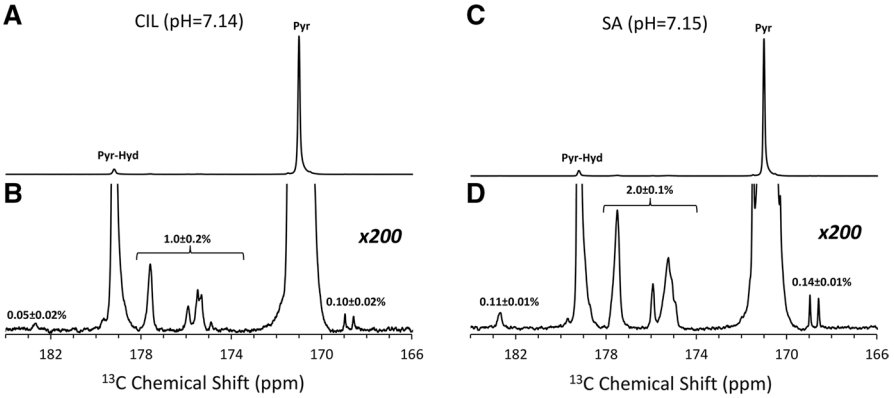

Fig. 3 ^{13}C-NMR spectra of hyperpolarized [1-^{13}C]pyruvate from two different suppliers showing the distribution of signal intensity attributed to impurities. The spectra shown here are the same as the spectra shown in Fig. 1. **a**, **b** Batch supplied by CIL, **b** is enlarged 200-fold. **c**, **d** Batch supplied by SA, **d** is enlarged 200-fold. For each batch the reported percentage of the different impurity signal(s) is the average ± standard deviation from the integrals calculated at the four different pH values

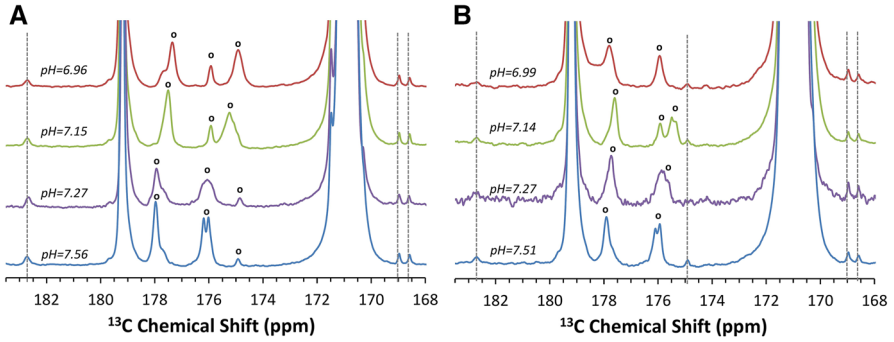

Fig. 4 Chemical shift pH dependence of impurity signals in two different batches of [1-^{13}C]pyruvic acid. Each spectrum is the sum of 15 acquisitions, summed between 10 and 80 s after arrival of hyperpolarized pyruvate to the probe, processed with a line broadening of 3 Hz. Impurity peaks whose chemical shift appear unchanged in the narrow pH range measured are marked with a dotted line while peaks whose chemical shift appears to be sensitive to the pH are marked with open circles. **a**, **b** ^{13}C spectra resulting from dissolutions of the hyperpolarized [1-^{13}C]pyruvic acid formulations prepared from batches purchased from SA and CIL, respectively. Only the chemical shift region of the impurities not overlapping the main [1-^{13}C]pyruvate signal is shown

(Fig. 4a, peaks marked with open circles). Similar results were observed with the CIL formulation (Fig. 4b). These results are reminiscent of the pH-dependent chemical shifts observed for the enol form of [1,5-^{13}C]zymonic acid [27] that appears to be one of the impurities observed here (Fig. 2).

Next we were interested in characterizing the longitudinal relaxation time of these impurities. We found that all of the observed impurities have T_1s above 30 s for the range of pH values studied. There did not appear to be significant differences in these T_1 values at different pH values (Fig. 5). Further, with the exception

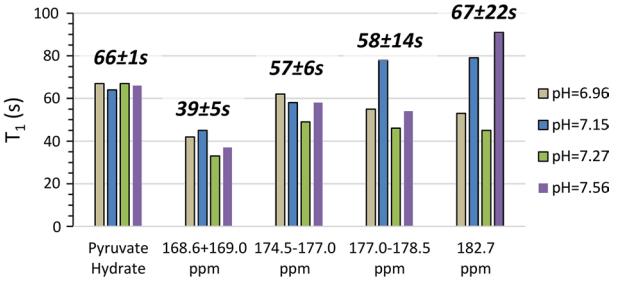

Fig. 5 T_1 values of pyruvate hydrate and the different impurities and impurity groups at varied pH values, with the average and standard deviation in the T_1 indicated above

of the impurity signals at 168.6 and 169.0 ppm, all impurity signals possess T_1s very similar to pyruvate, suggesting that they would be observed throughout the metabolic investigation of hyperpolarized [1-^{13}C]pyruvate.

As these impurity signals will make it difficult to discriminate metabolic products that are three to four orders of magnitude lower in concentration than pyruvate—even if there is sufficient sensitivity to observe them—it is important to develop techniques that reduce the amplitude of this impurity spectrum. We demonstrate that the amplitude of the impurity signals can be significantly reduced using a bloc of selective pulses—that selectively excite and depolarize the impurities while having a minimal effect on the pyruvate signal (Fig. 6a). Comparing the signals acquired 16 s apart—before and after the selective excitation bloc—it can be seen that the pyruvate signal is reduced by approximately 20% while the impurities' signals are reduced by more than 95%. If such an excitation bloc is applied in the beginning of a metabolic experiment, it will repress the impurities' signals while having only a small effect on the metabolite signals that are produced after the excitation bloc, as they originate from the still polarized [1-^{13}C] pyruvate. Interestingly, although the selective pulses also depolarize the pyruvate hydrate signal, in the non-selective acquisition observed after the selective excitation bloc its amplitude is only reduced ~50%. This can be understood as during the time between the end of the excitation bloc and the acquisition of the non-selective pulse (about 5 s), the hydrate's polarization is somewhat replenished due to chemical exchange with the still hyperpolarized [1-^{13}C]pyruvate.

The utility of such a sequence can be seen when studying the metabolism of hyperpolarized [1-^{13}C] pyruvate in a biological system. Here we demonstrate this utility in a system of ex vivo perfused viable rat brain slices. This set-up was developed in our lab and its utility for brain research is a topic of another study. Here we show that application of a bloc of four selective pulses with a repetition time of 1 s, successfully represses the impurity peaks while the peak of [1-^{13}C] lactate, continually formed from hyperpolarized [1-^{13}C]pyruvate is not suppressed and is detected with high signal-to-noise ratio (Fig. 7). As in the previous case, it can be seen that the peak of [1-^{13}C]pyruvate hydrate recovers somewhat after the bloc of selective excitation pulses, as it is in equilibrium with [1-^{13}C] pyruvate.

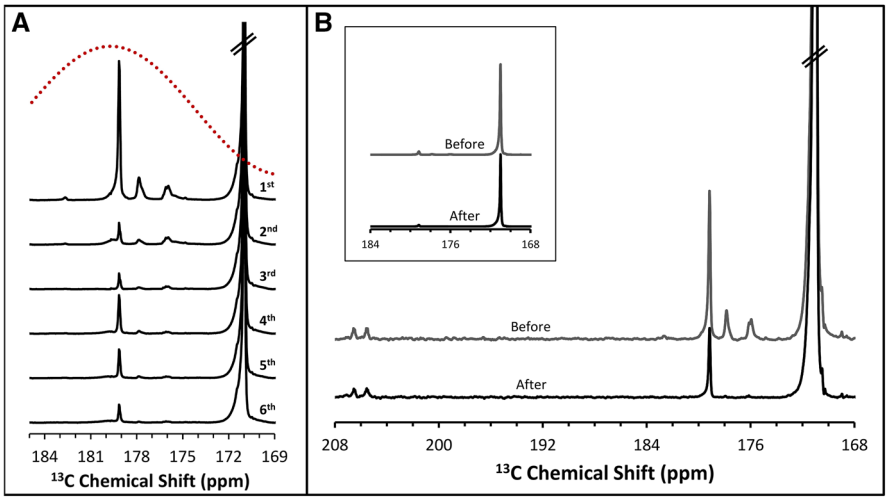

Fig. 6 ^{13}C spectra of a 14 mM solution of hyperpolarized [1-^{13}C]pyruvate. **a** The signals observed for a bloc of 6 selective pulses (sinc 2.5 ms) applied at 179 ppm every 0.5 s with the pyruvate signal truncated to allow for observation of the other signals. Above the spectra the excitation profile of the frequency selective pulse is shown, corresponding to ca. 90° excitation on [1-^{13}C]pyruvate hydrate and ca. 5° excitation on [1-^{13}C]pyruvate. **b** ^{13}C spectra observed before and after the selective excitation bloc applied in **a**. acquired with 10° broadband excitation. The upper signal was acquired 8 s before the acquisition of the 3 s excitation bloc while the lower signal was acquired 5 s after the final pulse in the excitation bloc. The pyruvate signals are truncated to allow observation of other signals but the full signal can be seen in the inset. The pyruvate signal decreased approximately 20% in the 16 s between the non-selective acquisitions while the impurity signal was reduced more than 95% and the hydrate signal was reduced ~50%

4 Discussion

Hyperpolarized [1-^{13}C]pyruvate is emerging as a powerful tool for metabolic NMR studies in living systems. The incredible sensitivity afforded by dDNP, allows the observation of metabolite signals that are 2–3 orders of magnitude smaller than the hyperpolarized pyruvate signal. However, the cost of such incredible sensitivity is that small impurities present in formulations of [1-^{13}C]pyruvic acid will now be observed. It can be appreciated that the chemical shifts of many of the sites that may be labeled upon metabolism of [1-^{13}C]pyruvate fall near or on the chemical shifts of impurities (Fig. 8).

It is important to note here that slight differences in the hyperpolarized solution pH due to variability in the dDNP process or in vivo pH heterogeneity could significantly change the impurity spectra, such that a control spectrum, acquired in the absence of metabolic activity, may not be sufficient to distinguish impurity and metabolite signals. Due to the long T_1s of all of the impurities that we observed in the relevant chemical shift range, this problem is expected to persist throughout the experimental window.

We demonstrated that by addition of a selective excitation bloc in the beginning of a hyperpolarized [1-^{13}C]pyruvate experiment, the signals of the impurities can

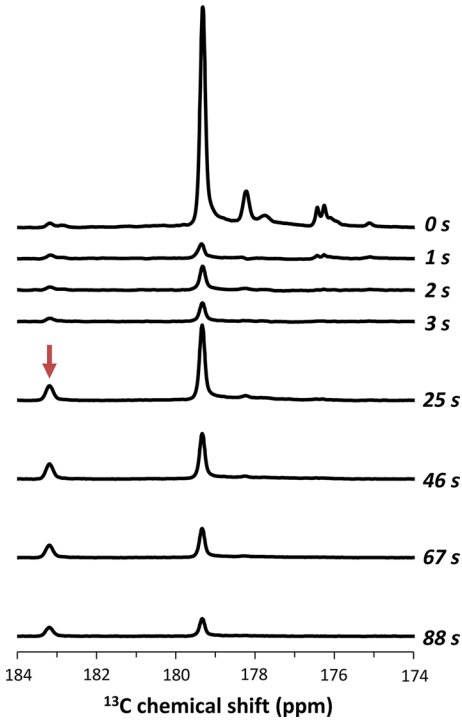

Fig. 7 ^{13}C NMR spectra acquired after addition of 14 mM hyperpolarized [1-^{13}C] pyruvate to brain slices. The spectra were acquired with selective excitation (sinc 3 ms) resulting in strong excitation of the 174–185 ppm region (> 45 °) and weak excitation of [1-^{13}C] pyruvate at 171.0 ppm. Four spectra were acquired with a repetition time of 1 s to fully saturate the impurity signals. Subsequent spectra were acquired every 21 s. The red arrow points to hyperpolarized [1-^{13}C]lactate produced in the brain cells from hyperpolarized [1-^{13}C]pyruvate

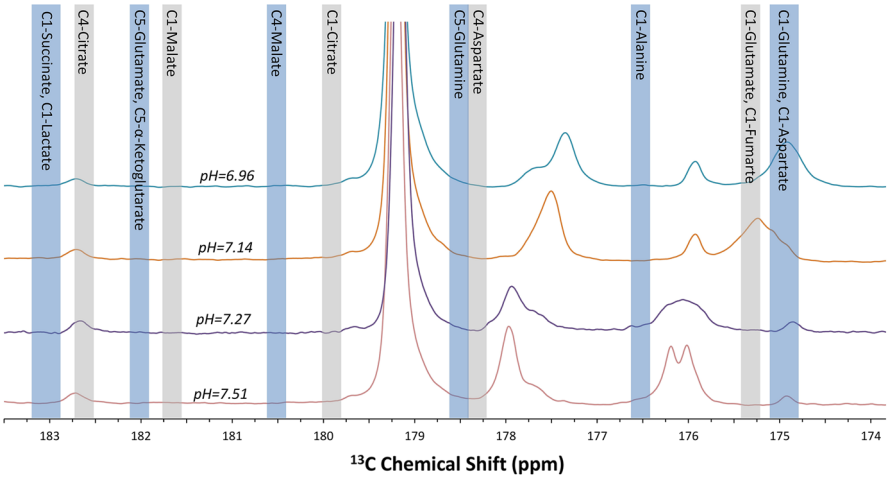

Fig. 8 Potential overlap between [1-^{13}C]pyruvate metabolite signals and the impurities' signals. The ^{13}C spectra shown here are the same as those presented in Fig. 4a. The chemical shift regions of potential [1-^{13}C]pyruvate metabolites are highlighted based on the chemical shifts reported in HMDB [31] with ±0.1 ppm

be reduced ≈20-fold while the signal of [1-^{13}C]pyruvate is only slightly affected. Then, the buildup of hyperpolarized metabolites in the same chemical shift regions can be monitored with an unperturbed baseline, i.e., without the background of the impurities' signals. The importance of such an approach is demonstrated in an ex vivo preparation consisting of perfused rat brain slices, where this technique enabled accurate evaluation of lactate production by the brain. Further studies on other biological systems using this technique are currently underway.

It is important to note that such a sequence represses the impurity signals, however, the impurities will still be present and their effect on the metabolic processes must be investigated. Studies have shown that parapyruvic acid inhibits the tricarboxylic acid cycle [32, 33], and although the toxicity of zymonic acid has been investigated [28] to the best of our knowledge, the metabolic effects of zymonic acid have not been studied.

5 Conclusion

We show the non-anecdotal appearance of hyperpolarized signals of impurities in two [1-^{13}C]pyruvic acid batches. The T_1 and the chemical shift pH dependence of these signals for a range of physiological pH values was studied and it is concluded that these impurity signals are likely to interfere with observation and interpretation of hyperpolarized pyruvate metabolism data due to their slow rate of longitudinal relaxation coupled with sensitivity of the chemical shift to slight changes in environmental pH. Finally, we demonstrated, both in solution and ex vivo—in perfused rat brain slices, that by applying frequency selective excitation pulses, the impurity signals can be significantly reduced with minimal effect on the signal of [1-^{13}C]pyruvate and—more importantly—the metabolic products subsequently produced from the [1-^{13}C]pyruvate. As the signals of metabolic products more than 100-fold lower in intensity than the signal of the hyperpolarized [1-^{13}C]pyruvate are routinely observed in living cells and in perfused organs [24, 34, 35], such a technique will be invaluable in such systems to reliably discriminate impurities from metabolic products and characterize the rate of formation of those products.

Funding Sponsor: This project has received funding from the European Research Council (ERC) under grant agreement No. 338040 to R.K-B) and from the European Union's Horizon 2020 research and innovation programme under grant agreement No. 667192.

Compliance with Ethical Standards

Conflict of Interest The authors declare that there is no conflict of interest regarding the publication of this paper.

References

1. J.H. Ardenkjaer-Larsen, B. Fridlund, A. Gram, G. Hansson, L. Hansson, M.H. Lerche, R. Servin, M. Thaning, K. Golman, Proc. Natl. Acad. Sci. USA. **100**, 10158–10163 (2003)
2. F.A. Gallagher, M.I. Kettunen, S.E. Day, D.-E. Hu, M. Karlsson, A. Gisselsson, M.H. Lerche, K.M. Brindle, Magn. Reson. Med. **66**, 18–23 (2011)
3. F.A. Gallagher, M.I. Kettunen, D.E. Hu, P.R. Jensen, R. in't Zandt, M. Karlsson, A. Gisselsson, S.K. Nelson, T.H. Witney, S.E. Bohndiek, G. Hansson, T. Peitersen, M.H. Lerche, K.M. Brindle, Proc. Natl. Acad. Sci. USA. **106**, 19801–19806 (2009)
4. A.P. Chen, J. Kurhanewicz, R. Bok, D. Xu, D. Joun, V. Zhang, S.J. Nelson, R.E. Hurd, D.B. Vigneron, Magn. Reson. Imaging **26**, 721–726 (2008)
5. S. Meier, M. Karlsson, P.R. Jensen, M.H. Lerche, J.O. Duus, Mol. Biosyst. **7**, 2834–2836 (2011)
6. K.R. Keshari, D.M. Wilson, A.P. Chen, R. Bok, P.E.Z. Larson, S. Hu, M. Van Criekinge, J.M. Macdonald, D.B. Vigneron, J. Kurhanewicz, J. Am. Chem. Soc. **131**, 17591–17596 (2009)
7. P.R. Jensen, S. Meier, J.H. Ardenkjaer-Larsen, J.O. Duus, M. Karlsson, M.H. Lerche, Chem. Commun. **34**, 5168–5170 (2009)
8. H. Allouche-Arnon, A. Gamliel, C.M. Barzilay, R. Nalbandian, J.M. Gomori, M. Karlsson, M.H. Lerche, R. Katz-Brull, Contrast Media Mol. Imaging **6**, 139–147 (2011)
9. H. Allouche-Arnon, A. Gamliel, J. Sosna, J.M. Gomori, R. Katz-Brull, Chem. Commun. **49**, 7076–7078 (2013)
10. F.A. Gallagher, M.I. Kettunen, S.E. Day, D.-E. Hu, J.H. Ardenkjaer-Larsen, R. in't Zandt, P.R. Jensen, M. Karlsson, K. Golman, M.H. Lerche, K.M. Brindle, Nature **453**, 940–943 (2008)
11. K. Golman, R. In 't Zandt, M. Thaning, Proc. Natl. Acad. Sci. USA **103** (30), 11270–11275 (2006)
12. S. Meier, P.R. Jensen, M. Karlsson, M.H. Lerche, Sensors **14**, 1576–1597 (2014)
13. M.K. Ravoori, S.P. Singh, J. Lee, J.A. Bankson, V. Kundra, Radiology **285**, 830–838 (2017)
14. S.J. DeVience, X. Lu, J. Proctor, P. Rangghran, E.R. Melhem, R. Gullapalli, G.M. Fiskum, D. Mayer, Sci. Rep. **7**, 1907 (2017)
15. A.J. Lewis, J.J. Miller, C. McCallum, O.J. Rider, S. Neubauer, L.C. Heather, D.J. Tyler, Diabetes **65**, 3544–3551 (2016)
16. C.H. Cunningham, J.Y.C. Lau, A.P. Chen, B.J. Geraghty, W.J. Perks, I. Roifman, G.A. Wright, K.A. Connelly, Circ. Res. **119**, 1177–1182 (2016)
17. S.J. Nelson, J. Kurhanewicz, D.B. Vigneron, P.E.Z. Larson, A.L. Harzstark, M. Ferrone, M. van Criekinge, J.W. Chang, R. Bok, I. Park, G. Reed, L. Carvajal, E.J. Small, P. Munster, V.K. Weinberg, J.H. Ardenkjaer-Larsen, A.P. Chen, R.E. Hurd, L.I. Odegardstuen, F.J. Robb, J. Tropp, J.A. Murray, Sci. Trans. Med. **5**, 198ra108 (2013)
18. I. Park, P.E.Z. Larson, J.W. Gordon, L. Carvajal, H.-Y. Chen, R. Bok, M. Van Criekinge, M. Ferrone, J. B. Slater, D. Xu, J. Kurhanewicz, D.B. Vigneron, S. Chang, S.J. Nelson, Magn. Reson. Med. **80**, 864–873 (2018)
19. E. Silverstein, P. Boyer, Anal. Biochem. **8**, 470–476 (1964)
20. R. Von Korff, Anal. Biochem. **8**, 171–178 (1964)
21. D. Groth, G. LePage, J. Am. Chem. Soc. **77**, 1681–1682 (1955)
22. R.W. von Korff, in *Purity and stability of pyruvate and α-ketoglutarate*, ed. J.M. Lowenstein in Methods in Enzymology: Citric Acid Cycle (Academic Press, New York, 1969), pp. 519–523
23. S. Margolis, B. Coxon, Anal. Chem. **58**, 2504–2510 (1986)
24. M.E. Merritt, C. Harrison, A.D. Sherry, C.R. Malloy, S.C. Burgess, Proc. Natl. Acad. Sci. USA. **108**, 19084–19089 (2011)
25. M. Marjanska, I. Iltis, A.A. Shestov, D.K. Deelchand, C. Nelson, K. Ugurbil, P.G. Henry, J. Magn. Reson. **206**, 210–218 (2010)
26. B. Pullinger, H. Profka, J.H. Ardenkjaer-Larsen, N.N. Kuzma, S. Kadlecek, R.R. Rizi, NMR Biomed. **25**, 1113–1118 (2012)
27. C. Hundshammer, S. Duwel, S.S. Kocher, M. Gersch, B. Feuerecker, C. Scheurer, A. Haase, S.J. Glaser, M. Schwaiger, F. Schilling, ChemPhysChem **18**, 2422–2425 (2017)
28. S. Duwel, C. Hundshammer, M. Gersch, B. Feuerecker, K. Steiger, A. Buck, A. Walch, A. Haase, S.J. Glaser, M. Schwaiger, F. Schilling, Nat. Commun. **8**, 15126 (2017)
29. R.J. Perkins, R.K. Shoemaker, B.K. Carpenter, V. Vaida, J. Phys. Chem. A **120**, 10096–10107 (2016)

30. D. Massiot, F. Fayon, M. Capron, I. King, S. Le Calvé, B. Alonso, J.-O. Durand, B. Bujoli, Z. Gan, G. Hoatson, Magn. Reson. Chem. **40**, 70–76 (2002)
31. D.S. Wishart, T. Jewison, A.C. Guo, M. Wilson, C. Knox, Y. Liu, Y. Djoumbou, R. Mandal, F. Aziat, E. Dong, S. Bouatra, I. Sinelnikov, D. Arndt, J. Xia, P. Liu, F. Yallou, T. Bjorndahl, R. Perez-Pineiro, R. Eisner, F. Allen, V. Neveu, R. Greiner, A. Scalbert, Nucleic Acids Res. **41**, D801–D807 (2013)
32. E.J. Davis, BBA-Bioenergetics **143**, 26–36 (1967)
33. C.M. Montgomery, A.S. Fairhurst, J.L. Webb, J. Biol. Chem. **221**, 369–376 (1956)
34. I. Park, J. Mukherjee, M. Ito, M.M. Chaumeil, L.E. Jalbert, K. Gaensler, S.M. Ronen, S.J. Nelson, R.O. Pieper, Can. Res. **74**, 7115–7124 (2014)
35. K.R. Keshari, R. Sriram, M. Van Criekinge, D.M. Wilson, Z.J. Wang, D.B. Vigneron, D.M. Peehl, J. Kurhanewicz, Prostate **73**, 1171–1181 (2013)